RESEARCH ARTICLE

Macromolecular Materials and Engineering
Open Access
www.mame-journal.de

Melt-Processable and Electrospinnable Shape-Memory Hydrogels

Turdimuhammad Abdullah, Cagatay Altınkok, and Oguz Okay**

Due to their ability to adapt to subtle changes in response to various external and internal stimuli, smart hydrogels have become increasingly popular in research and industry. However, many currently available hydrogels suffer from poor processability and inferior mechanical properties. For example, the preparation of a hydrogel network that can be subjected to melt processing and electrospinning is challenging. Herein, a series of mechanically strong, shape-memory hydrogels based on polyacrylic acid (PAAc) chains containing 20–50 mol% of crystallizable n-octadecylacrylate (C18A) segments are prepared by an organosolv method followed by in situ physical cross-linking via hydrophobic interactions. The hydrogels exhibit a reversible strong to weak gel transition at 50–60 °C and can be melt-processed at 60–100 °C, depending on the molar fraction of C18A. Additionally, the hydrogels can be dissolved in chloroform/ethanol mixture to form a viscous solution, which can then be used to produce a nanofibrous network by electrospinning. Effects of polymer concentration, volume ratio of solvents, and mole fraction of C18A on electrospinning are investigated to produce smooth, uniform nanofibers with small fiber diameter. The produced nanofibers, while maintaining their chemical structure, show significantly improved water adsorption capacity, enhanced mechanical properties, and fast shape-memory performance.

1. Introduction

There is a burgeoning interest in intelligent materials capable of altering their form and physiochemical attributes in response to specific stimuli, including but not limited to temperature, light, pH, or magnetic fields.[1,2] These materials have captured the attention of both the research community and industry due to their diverse applications in fields such as biomedical engineering, aerospace engineering, sensors, and the textile industry.[3–5] Within the domain of polymer-based smart materials, two prominent categories stand out: smart hydrogels and shape-memory polymers (SMPs).[6,7] Notably, hydrogels are particularly favored for biomedical applications due to their inherent tissue-like physiochemical structure, impressive moisture absorption capacity, and exceptional permeability.[8,9] In contrast, SMPs typically exhibit significantly swifter response times, greater fixability and recovery ratios, and more robust mechanical properties when compared to hydrogels.[6,7] Consequently, over the past decade, there has been a concerted and extensive research effort directed toward the development of shape-memory hydrogels (SMHs) that combine the advantageous properties of both hydrogels and SMPs.[7,10]

One of the most established approaches for the creation of SMHs hinges on the utilization of hydrophobic interactions.[8,11] This entails the incorporation of crystallizable hydrophobic segments acting as a reversible cross-linker into hydrophilic polymer chains.[12,13] To illustrate, we have developed SMHs based on polyacrylic acid (PAAc), incorporating n-octadecyl acrylate (C18A) as the hydrophobic segment through micellar copolymerization techniques.[10,14] These P(AAc-co-C18A) hydrogels offer not only high mechanical stiffness, customizable thermomechanical properties, and remarkable fixity and recovery ratios but also possess the exceptional characteristic of melt-processability. In other words, when exposed to a temperature above the melting point of the crystalline C18A domains, the hydrogel can be effortlessly formed into desired shapes by injection molding and/or extrusion. Nonetheless, it is worth noting that the inclusion of the hydrophobic domain in the hydrogel substantially diminishes its water absorption capacity.[15,16] Moreover, SMHs generated through random polymerization and crosslinking fail to provide the controlled microstructure essential for specific applications, such as the precise distribution of pore sizes and porosity, which are of paramount significance in numerous applications, such as biomedical applications, membrane technology, and textile industry.[17,18]

T. Abdullah, C. Altınkok, O. Okay
Department of Chemistry
Istanbul Technical University
Maslak, Istanbul 34469, Turkey
E-mail: abudulat@itu.edu.tr; okayo@itu.edu.tr
T. Abdullah
İzel Kimya Research and Development Center
Dilovası, Kocaeli 41455, Turkey
T. Abdullah
Stem Cell and Tissue Engineering Application and Research Center
İstinye University
İstanbul 34010, Turkey

The ORCID identification number(s) for the author(s) of this article can be found under https://doi.org/10.1002/mame.202400166

DOI: 10.1002/mame.202400166

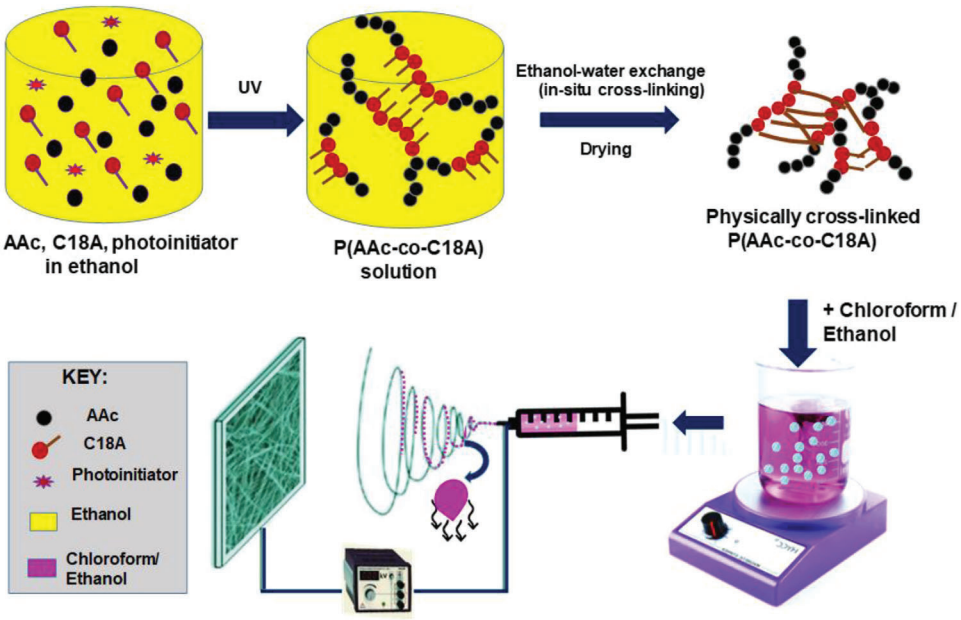

Figure 1. Schematic illustration depicting the synthesis of melt-processable PAAc hydrogels containing C18A units via the organosolv method, followed by a solvent exchange to induce physical cross-linking, and finally electrospinning to generate a nanofibrous network.

In spite of the various technological approaches, electrospinning has proven to be one of the forefront techniques to offer precise control over the porosity and pore size of hydrogels.[17,19] In this approach, a high-voltage electric field is applied upon a viscous polymer solution or melt, resulting in the formation of a nanofiber network.[20] The fiber dimensions and pore structure of electrospun hydrogels can be deliberately adjusted through the regulation of electrospinning process parameters (e.g., the applied voltage and feed rate) in conjunction with the properties of the polymer solution used.[21–23] The nanofibrous microstructure of electrospun hydrogels yields a high surface area-to-volume ratio, which not only fosters cellular adhesion and interactions but also facilitates the absorption of moisture and various chemical substances.[24,25] Furthermore, electrospun hydrogels often exhibit enhanced mechanical strength in comparison to conventional hydrogels.[17,26] This increased strength is especially advantageous for applications that involve bearing substantial loads.

In this study, we synthesized a series of melt-processable, shape-memory hydrogels by incorporating 20–50 mol% of crystallizable C18A segments within PAAc network using an organosolv method, followed by in situ physical cross-linking via hydrophobic interactions. Notably, these hydrogels exhibit a reversible transition between strong and weak gel state at temperatures ranging from 50 to 60 °C. Furthermore, they can be effectively melt-processed within the temperature range of 60 to 100 °C, with the specific temperature varying according to the molar fraction of C18A. Moreover, our synthesized hydrogels demonstrate the ability to dissolve in a mixture of chloroform and ethanol, forming a viscous solution. This solution can be utilized to produce a nanofibrous network through electrospinning (**Figure 1**). Our investigation into the electrospinning process considered key parameters such as polymer concentration, voltage, volumetric ratios of solvents, and the molar fraction of C18A. Through optimization, we achieved the production of nanofibers that are smooth, uniform, and possess the smallest possible fiber diameters. The resulting nanofibers exhibit remarkable enhancements in water adsorption capacity, mechanical properties, and a high shape-recovery rate while maintaining their chemical structure. This innovative approach holds significant promise for designing hydrogels with versatile dynamic behaviors and processability. These findings open up new avenues for expanding the applications of such hydrogels in various fields.

2. Results and Discussion

In our previous report, we synthesized P(AAc-co-C18A) hydrogels by micellar copolymerization of hydrophilic acrylic acid (AAc) monomer with 20–50 mol% crystallizable, hydrophobic C18A comonomer, where the latter was solubilized in worm-like sodium dodecyl sulfate (SDS) micelles.[10] The prepared hydrogels displayed many interesting characteristics such as self-healing ability, robust mechanical properties, and shape-memory effects in a moderate temperature range. However, the synthesis process of the hydrogel by this route is relatively complex and it takes more than a month to remove the surfactant from the hydrogels.[10] Additionally, SDS used in this work as a surfactant is generally regarded as toxic.[27] Therefore, in the present work, we use a simple organosolv method to synthesize the above-mentioned hydrogels. In this method, C18A was first dissolved in ethanol prior to mixing with AAc, then the monomers were copolymerized at room temperature (23 ± 2 °C) under UV irritation using Irgacure 2959 as an initiator. The total concentration of the monomers for this process was fixed at 3 M, and the molar fraction of C18A was varied between 20% and 50%. For example, 3.41 g of C18A, 4.66 mL of ethanol, 1.34 mL of AAc, and 14.3 mg of Irgacure 2959 were used to prepare P(AAc-co-C18A) gels with 35 mol% of C18A. The formed gels were found to be at a liquid state above 40 °C that enables them to be molded into any

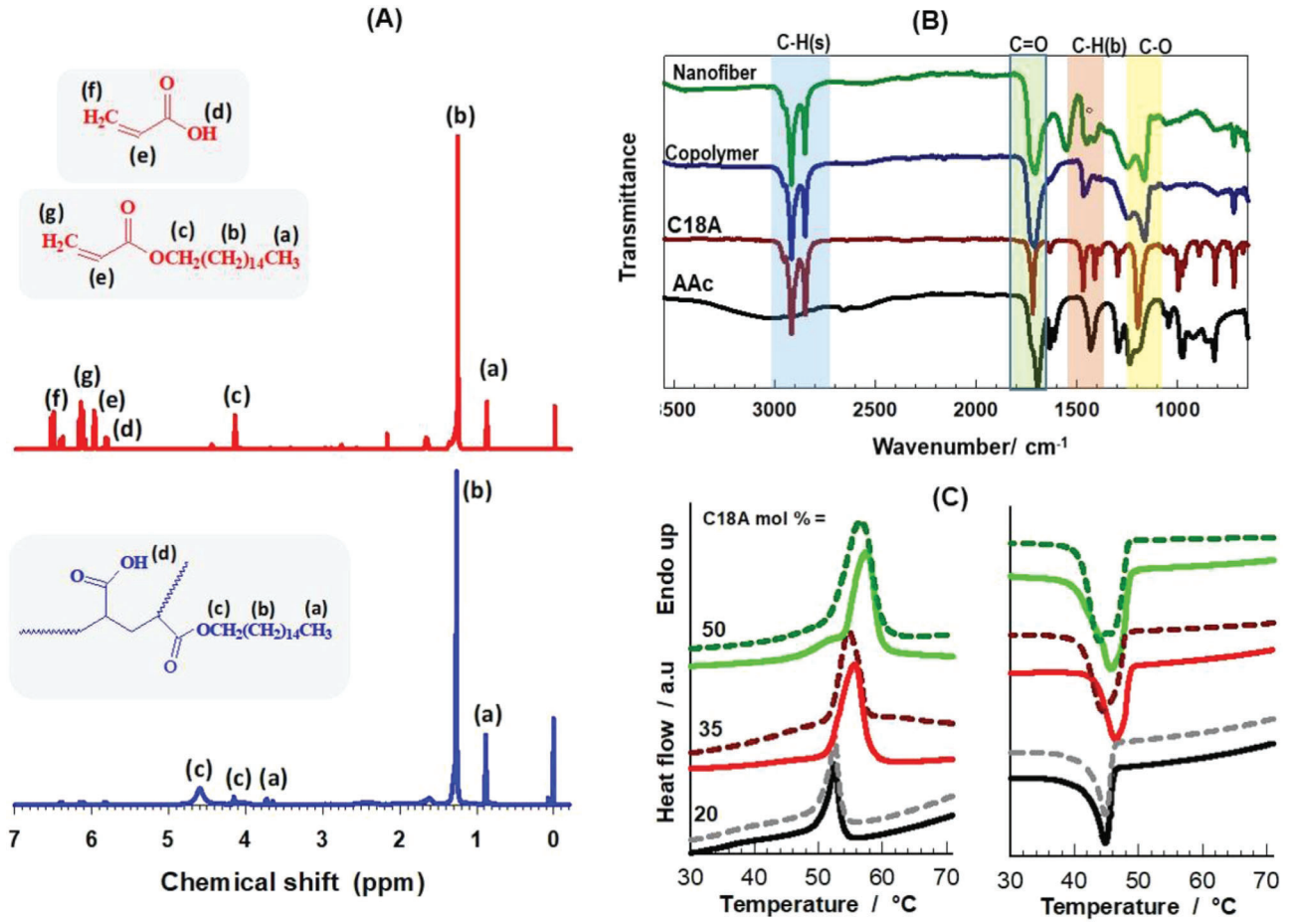

Figure 2. A) ^{1}H NMR spectra of AAc/C18A monomer mixture (upper panel), and P(AAc-co-C18A) hydrogel (bottom panel), both containing 35 mol% C18A. B) FTIR spectra of as-synthesized and electrospun P(AAc-co-C18A) hydrogels containing 35 mol% of C18A. The spectra of AAc and C18A monomers are also shown in the figure. C) Heating and cooling DSC spectra of as-synthesized (solid curves) and electrospun hydrogels (dashed curves) with different molar fractions of C18A as indicated.

shape. Afterward, the gels were immersed in a large volume of water for two days. During this process, ethanol in the hydrogel network replace with water and hence, strong hydrophobic interactions could be created between the octadecyl side chains of C18A units enabling the formation of a supramolecular P(AAc-co-C18A) hydrogels.[28]

The formation of the copolymer from a mixture of AAc and C18A monomers was confirmed by nuclear magnetic resonance (NMR) spectroscopy analysis. **Figure** 2A shows ^{1}H NMR spectra of AAc/C18A monomer mixture (upper panel), and P(AAc-co-C18A) hydrogel (bottom panel), both containing 35 mol% C18A. The characteristic peaks are observed at 1.3 ppm, corresponding to the $-CH_2$-proton, at 4.4 and 4.0 ppm, corresponding to the $-OCH_2$-proton, and at 0.9 and 3.6 ppm, corresponding to the $-CH_3$ proton.[29,30] Furthermore, the presence of C=C double bonds along with their corresponding functional groups is indicated by the presence of characteristic peaks between 6 and 6.6 ppm in the monomer mixture.[7,30] The absence of these peaks in the copolymer spectrum, as expected, is a clear indication of the effective conversion of monomer units into polymer chains and confirms the successful polymerization. The chemical structure of the synthesized P(AAc-C18A) hydrogels was analyzed using FTIR spectroscopy (Figure 2B). In the spectra, distinctive absorption peaks were identified at 1697 cm^{-1} (C=O stretching) and 1240 cm^{-1} (C—O stretching) indicating the presence of polymerized AAc segments within the copolymer hydrogel.[11] Simultaneously, corresponding absorption bands for the polymerized C18A segment were evident at 1730 cm^{-1} (C=O stretching), 1150 cm^{-1} (C—O stretching), 1470 cm^{-1} (CH bending), 2855 cm^{-1} (CH bond), and 2920 cm^{-1} (CH bond).[30] Furthermore, absorption bands at 1632 and 985 cm^{-1}, corresponding to C=C and $=CH_2$, were observed in acrylic acid (AAc) and C18A monomers. However, these bands disappeared in the copolymer, an indication of the effective conversion of vinyl double bonds during radical polymerization.[31] This spectroscopic analysis provides a clear characterization of the chemical composition, confirming the successful incorporation of both AAc and C18A segments into the hydrogel structure. X-ray diffraction (XRD) analysis of P(AAc-co-C18A) hydrogels reveals a significant correlation between the molar fraction of C18A and a diffraction peak observed at ≈21.5° corresponding to a d-spacing of 0.41 nm revealing hexagonal packing of side C18 chains (Figure S1, Supporting Information).[10] The increasing sharpness of the peak with higher molar fractions of C18A indicates that as the

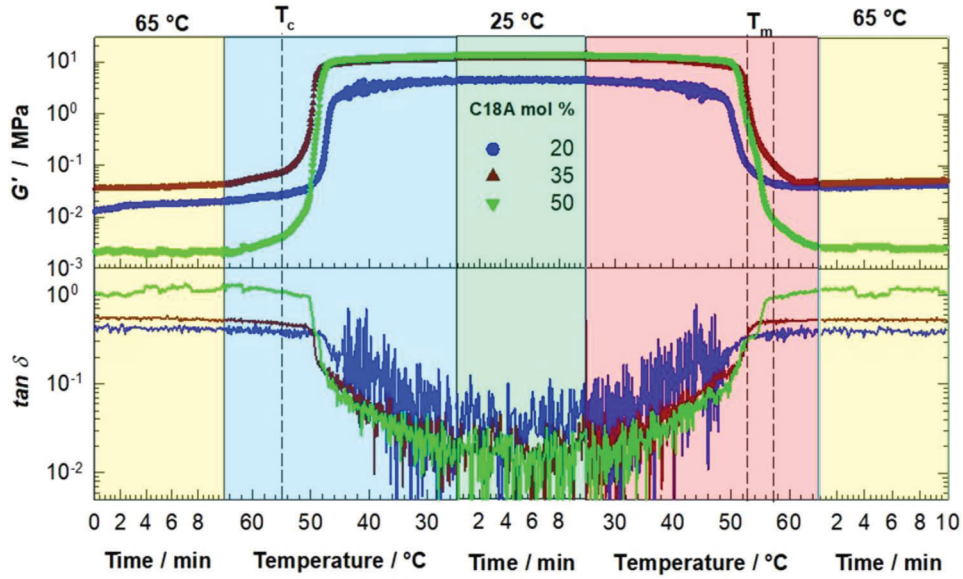

Figure 3. The changes in the storage modulus G' and the loss factor tan δ of PAAc hydrogels with varying C18A mole fractions during a cooling-heating cycle ranging from 25 to 65 °C. The cycle is composed of five steps, indicated by different background colors. The first step is isothermal oscillation at 65 °C for 10 min. The second step is cooling down from 65 to 25 °C at a rate of 1 °C min^{-1}. The subsequent step is isothermal oscillation at 25 °C for 10 min. This is followed by heating up from 25 to 65 °C at a rate of 1 °C min^{-1}, after which the process is repeated with isothermal oscillation at 65 °C for 10 min. The melting (T_m) and crystallization (T_c) temperature ranges of the hydrogels are marked by vertical dashed lines. C18A = 20 (blue circle), 35 (dark red triangle up), and 50 mol% (green triangle down). Frequency = 1 Hz. Strain amplitude = 0.1%.

proportion of C18A increases, the degree of crystallinity within the hydrogel also increases. This is likely due to the enhanced alignment and interaction of the C18A side chains, leading to more defined and ordered crystalline structures.[32]

The phase transition behavior of the swollen hydrogels as response to temperature due to the presence of crystalline hydrophobic C18A domains was evidenced by DSC. Figure 2C shows heating and cooling DSC scans of as-prepared (solid curves) and electrospun P(AAc-co-C18A) hydrogels (dashed curves) with 20, 35, and 50 mol% C18A. All the hydrogels display distinct melting and crystallization peaks. The melting temperature (T_m) of the hydrogels is between 52.5 and 57.5 °C, that generally increases with increasing mole fraction of C18A while their crystallization temperature (T_c) is around 45–46 °C regardless of the hydrogel composition. A similar trend was also reported in the literature.[10]

The temperature dependent thermomechanical properties of the synthesized hydrogels were investigated by an oscillatory temperature-sweep test. All the hydrogels exhibited clear reversible changes in the storage modulus G' between below and above their melting temperature (**Figure 3**). The most drastic changes were observed for the hydrogels with 50 mol% of C18A, in which G' was maintained at ≈11.5 MPa when the temperature was below 50 °C and it dropped by ≈1200-fold to ≈9.3 kPa at the melting temperature of the crystallizable C18A domain (57.5 °C). Similar changes can be seen in the value of the loss factor tan δ. All hydrogels are in a solid-like state below their melting temperature, i.e., tan δ < 0.1.[10] Then, there is a reversible strong-to-weak gel transition when the temperature is above the melting point during which tan δ increases from below to above 0.1.[10,14] Further, the hydrogel with 50 mol% of C18A even showed a liquid state when the temperature was 65 °C (tan $\delta > 1$).[10] Overall, the synthesized hydrogels show reversible strong-to-weak gel transition above the melting temperature of C18A crystalline domain.

The melt-processability of the hydrogels was evaluated by studying their rheological behavior above their melting temperature using a frequency-sweep test at various temperatures. A conical plate (40 mm and 4°) was used for this measurement, which is more adequate for molten/liquid samples.[33] **Figure 4** presents the frequency dependences of the complex viscosity (upper panel) and tan δ (bottom panel) of P(AAc-co-C18A) hydrogels containing a) 20, b) 35, and c) 50 mol% C18A at different temperatures. The arrows indicate the direction of increasing temperature. All the hydrogels generally exhibited a shear-thinning behavior and the viscosity significantly decreased while tan δ increased with increasing temperature. The hydrogels with a higher C18A content showed a lower solid–liquid phase transition temperature and lower viscosity, due to the ascendancy of the crystalline domain. For example, at 65 °C, the hydrogel with 50 mol% of C18A displays 20–200 Pa s^{-1} viscosity and the loss factor is above unity.[34] Therefore, it can be extruded through a syringe by raising the temperature above 65 °C. In contrast, however, the extrusion temperature should be higher than 85 °C and the feed speed must be also high enough to extrude the hydrogel if the molar fraction of C18A is lower than 35%. This could be owing to the fact that a higher density of the crystalline domain facilitates the phase transition of hydrogels at a lower temperature.[10,35]

Next, we assessed possibility to fabricate nanofibrous membrane from the synthesized hydrogels using electrospinning technique. We dissolved the dried hydrogels in the mixture of chloroform and ethanol to create homogeneous viscoelastic solution. Several key electrospinning parameters were optimized to obtain a smooth and uniform fibrous structure with small

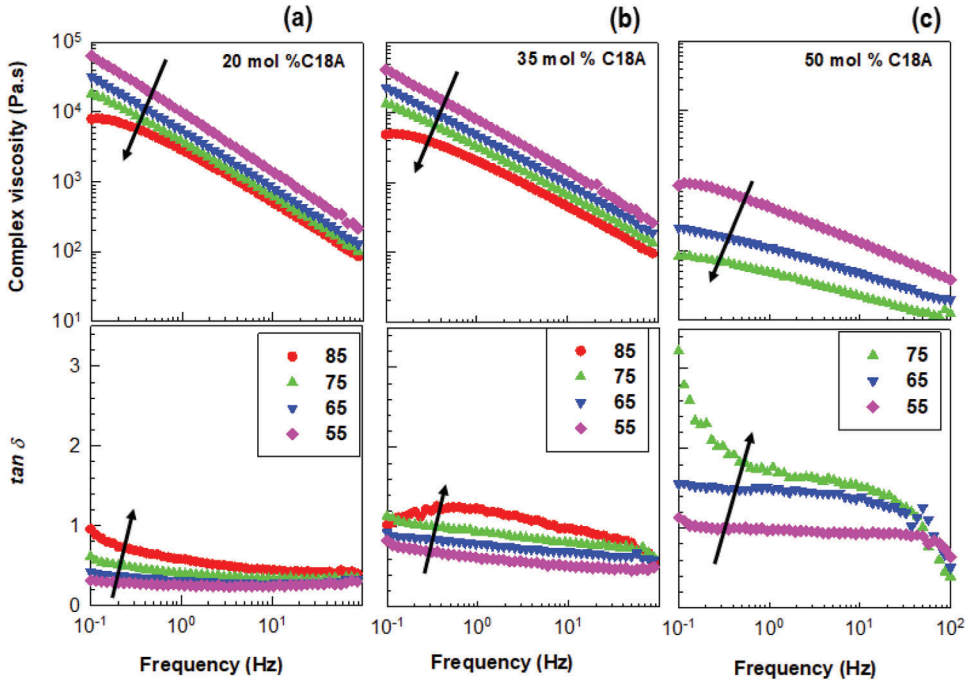

Figure 4. The frequency-dependent variations of complex viscosity and loss factor tan δ of P(AAc-co-C18A) hydrogels containing a) 20, b) 35, and c) 50 mol% C18A at different temperatures as indicated. The arrows indicate the direction of increasing temperature.

fiber diameters. We found that polymer concentration and solvent ratio are the most critical factors to influence fiber size and morphology among them. For instance, a lower polymer concentration is recommended to smallen the fiber diameter by reducing deformation resistance of the polymeric solution.[36] Whereas, when the polymer concentration is less than 20 wt% (e.g., 15 wt%), it promotes the development of beads within fibers due to insufficient polymer chain entanglement and excessive surface tension (Figure S2, Supporting Information).[37] Among the solvents, high volumetric fraction of ethanol was found to encourage formation of smaller fiber size, due to its much higher dielectric constant than chloroform (25.3 vs 4.81).[38,39] Furthermore, the lower volatility of ethanol (vapor pressure at 25 °C is ≈7.87 kPa[40]) compared to chloroform (26.54 kPa[40]) during the electrospinning process allows the jet to stretch under the electric field for more time before solidifying, helping to form thinner fibers. However, the hydrogels could not be dissolved if the ethanol: chloroform volumetric ratio is higher than 2:1. Overall 20 wt% of polymer concentration, a mixture of chloroform and ethanol in a volumetric ratio of 1:2, 1 mL h^{-1} of feed rate, 17 kV of voltage, and 13 cm of needle-collector distance was found to be the optimum conditions for electrospinning the P(AAc-co-C18A) hydrogels (Figure S3, Supporting Information).

The effect of the molar fractions of C18A on the morphology of electrospun P(AAc-co-C18A) hydrogels is shown in **Figure 5**. The generated P(AAc-co-C18A) fiber was found to be smooth and no beads existed on the fiber regardless of the molar fractions of C18A. However, P(AAc-co-C18A) hydrogels containing a higher molar fraction of C18A generated considerably larger fibers. For instance, the fiber size increased from 887 ± 96 to 1194 ± 210 nm when the molar fraction of C18A raised from 20 to 50 mol%. This intriguing transformation can be ascribed to the higher inter-chain interactions within copolymers in the presence of a higher amount of long-chain C18A segments.[41,42] Namely, the increase in C18A content fosters stronger intermolecular connections, thereby leading to the expansion of fiber dimensions.

We compared the chemical structure and thermal behavior of the electrospun nanofibrous hydrogels with as-prepared hydrogels through FTIR and DSC analysis and found that these properties were not altered by electrospinning (Figure 2B,C). However, remarkable changes in terms of swelling capacity and mechanical properties have been observed for P(AAc-co-C18A) hydrogels after electrospinning. For example, the swelling ratio (SR) of P(AAc-co-C18A) hydrogels was between 1.25 and 2.0 that decreases with increased molar fractions of C18A, e.g., SR = 2.0 ± 0.1, 1.40 ± 0.02, and 1.25 ± 0.01 for the hydrogels with 20, 35, and 50 mol% of C18A, respectively. In contrast, electrospun nanofibers show a nearly fourfold increase in SR compared to their as-prepared counterparts (**Figure 6a**). The hydrogel with 20 mol% of C18A, for instance, had its SR raised from 2.0 to 8.1 after electrospinning. The enhanced swelling behavior of nanofibrous hydrogels is due to their high surface area-to-volume ratio facilitating greater water penetration and allowing better interactions with water during the swelling process.[43,44] Additionally, the porous morphology of nanofiber structures, along with interconnected voids and channels, provides additional pathways for water diffusion.[45] Furthermore, capillary forces, induced by small pore sizes and high aspect ratios, enhance water transport into the nanofiber matrix.[46]

In terms of mechanical property, as-prepared hydrogels were brittle and could not be subjected to tensile testing. While we were able to perform tensile testing on the electrospun P(AAc-co-C18A) nanofibrous hydrogels. Figure 6b,c illustrates the tensile stress-strain curves, along with the changes in Young's modu-

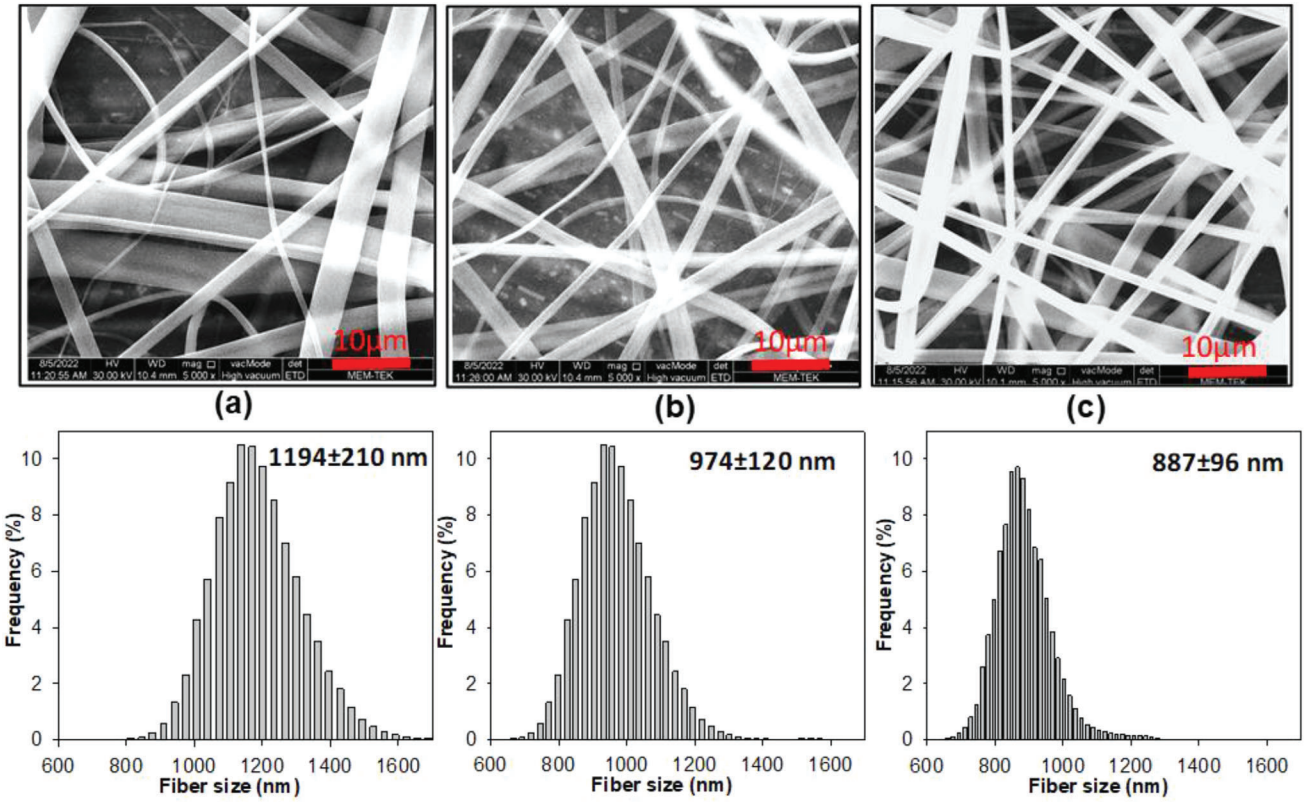

Figure 5. The SEM micrograph and fiber size distribution of electrospun P(AAc-co-C18A) hydrogels containing a) 50, b) 35, and c) 20 mol% of C18A.

lus (E), stress at fracture (σ_f), and strain (ϵ_f) for the electrospun P(AAc-co-C18A) hydrogels with different C18A molar fractions (f_{C18A}). Increasing f_{C18A} leads to a decrease in both E and σ_f while the changes in the strain ϵ_f are proportional to f_{C18A}. For instance, electrospun P(AAc-co-C18A) hydrogel with 50 mol% C18A displayed significantly higher flexibility (52 ± 1%) but a low modulus (1.0 MPa) compared to the one with 20 mol% of C18A (20 ± 1% strain and 2.2 MPa modulus). This trend could be caused by the morphological structure of the electrospun hydrogels that a smaller fibrous network typically has a higher surface area-to-volume ratio, which can increase their stiffness.[47] On the other hand, a larger fibrous network has a lower surface area-to-volume ratio, which can contribute to enhanced flexibility.[48]

Moreover, the electrospun hydrogels exhibited excellent shape-memory behavior with shape-fixity and shape-recovery ratios of 95–98 and 91–93%, respectively. However, they demonstrated a slightly lower shape-recovery and shape-fixity compared to the bulk hydrogels, which was attributed to reduced intermolecular interactions between the AAc and C18A segments during electrospinning (Figure 6d,e). Nevertheless, the shape-recovery speed of the electrospun hydrogels was significantly faster than that of their bulk hydrogel counterparts. While it took 20–30 s for the bulk hydrogels to recover their original shapes, the electrospun hydrogels achieved complete recovery in less than 5 s (Figure 6f,g, Video S1, Supporting Information). This faster shape-recovery rate could be attributed to nanofibrous structure of the electrospun hydrogels that provide a larger surface area-to-volume ratio, allowing for more efficient interaction with external stimuli, which can trigger the shape-recovery process.[49] Additionally, the porous nature of electrospun nanofibers enhances the diffusion of stimuli throughout the hydrogel matrix, resulting in faster response times compared to dense bulk hydrogels where diffusion may be slower.[49,50] Finally, XRD analysis indicated that electrospun fibers exhibited a higher degree of intensity in their peaks compared to their bulk counterparts (Figure S1, Supporting Information). This can be attributed to the high degree of orientation and crystallinity that may contribute to enhanced shape-memory properties.[51] This is because the ordered structure can facilitate more rapid and efficient reorganization of polymer chains during shape-recovery.[52] Overall, high surface area, highly interconnected porous structure, and aligned polymer chains are driving factor for the electrospun hydrogels to promote faster shape-recovery kinetics compared to traditional bulk hydrogel materials.

3. Conclusion

We have successfully synthesized a series of melt-processable, shape-memory hydrogels made of PAAc containing 20–50 mol% C18A segments using an organosolv method. The hydrogels displayed a reversible transition from a strong to a weak gel state within a temperature range of 50–60 °C. They also demonstrated efficient melt-processing abilities at temperatures ranging from 60 to 100 °C, with the specific temperature varying based on the molar fraction of C18A. Additionally, the hydrogels that were synthesized had the ability to create a viscous solution suitable for

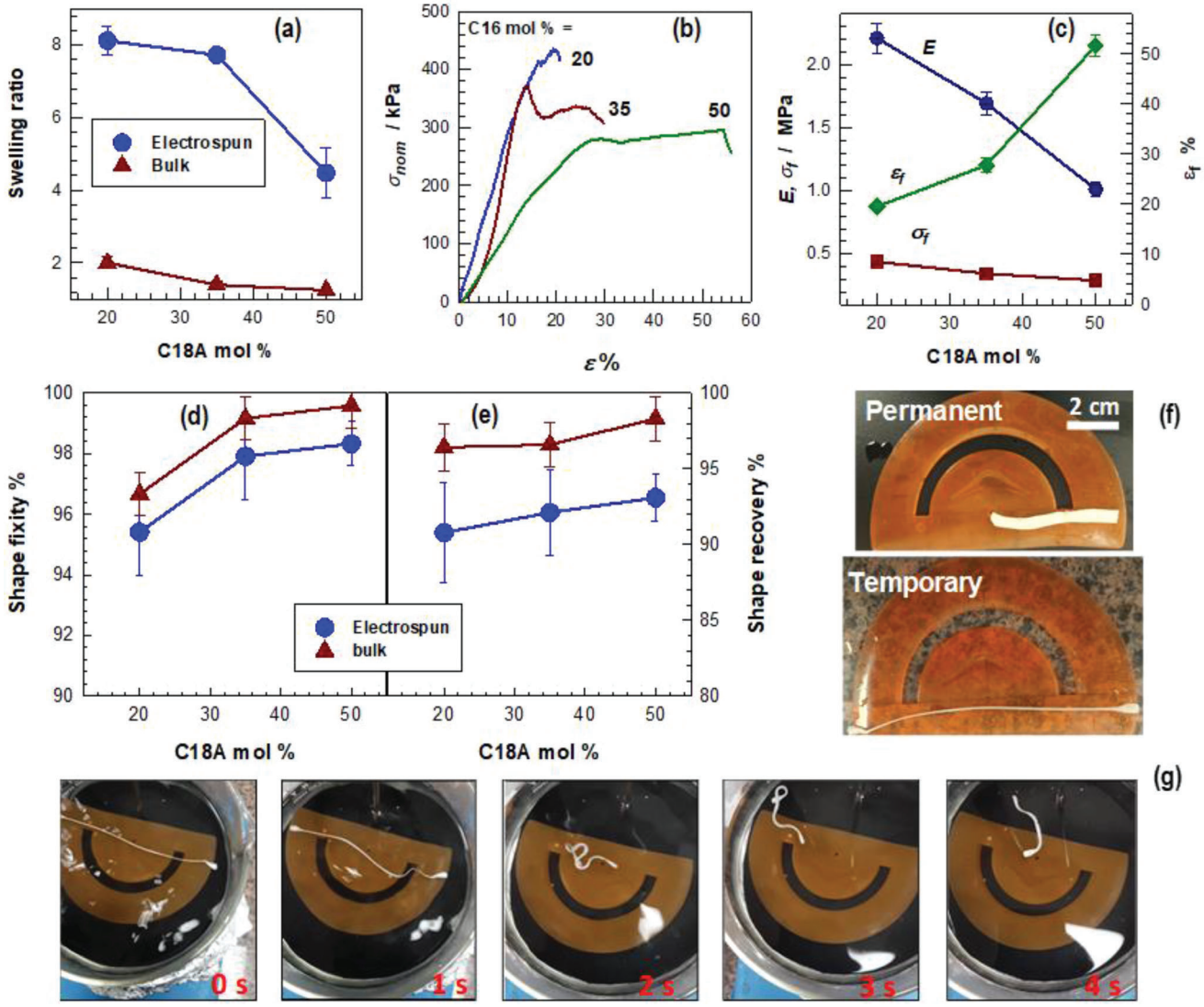

Figure 6. a) The swelling ratio (SR) of the as-synthesized (bulk) and electrospun hydrogels with different molar fractions of C18A. b) The tensile strain–stress curves of electrospun hydrogels with different molar fractions of C18A. c) Young's modulus E, stress at break σ_f, and elongation at break ϵ_f of the electrospun hydrogels with different C18A mol%. d) Shape-fixity and e) shape-recovery ratios of the as-synthesized (bulk) and electrospun hydrogels with different molar fractions of C18A. f) Permanent and temporary shapes of the electrospun hydrogel with 50 mol% C18A. g) Shape-recovery process of an electrospun hydrogel in water at 65 °C. C18A = 50 mol%. The recovery times are indicated.

electrospinning into a nanofibrous network. The nanofibers exhibited significant improvements in water adsorption capacity, mechanical properties, and shape-memory rate, while maintaining their chemical structure. Overall, this innovative approach has potential for designing hydrogels with versatile dynamic behaviors and processability, opening new avenues for their application across various fields.

4. Experimental Section

Preparation of P(AAc-co-C18A) Hydrogels: *N*-octadecyl acrylate (C18A), 2-hydroxy-4′-(2-hydroxyethoxy)-2-methylpropiophenone (Irgacure 2959), chloroform, ethanol, and an alumina column were supplied by Sigma-Aldrich. Acrylic acid (AAc, Merck) was treated with an alumina column (Sigma-Aldrich) to remove its inhibitor. The AAc-C18A monomer solution in ethanol, containing 20–50 mol% C18A, was prepared by melting C18A at 40 °C on a magnetic stirrer, then sequentially adding ethanol and AAc. After adding 0.2 w/v% Irgacure 2959 photoinitiator, the solution was transferred to a 10 mL syringe and exposed to UV light at 365 nm wavelength for 24 h for photopolymerization. The samples were subsequently immersed in water for two days to induce physical crosslinking, resulting in the formation of P(AAc-co-C18A) hydrogels.

Electrospinning: P(AAc-co-C18A) hydrogels were dried and then dissolved in a mixture of chloroform and ethanol by stirring for 3 h at 23 ± 2 °C. The solution was then transferred to a 5-mL syringe connected to an 18-gauge blunt metallic needle for electrospinning. Electrospinning parameters were systematically studied for the P(AAc-co-C18A) hydrogels with 35 mol% of C18A to obtain optimal electrospinning conditions for bead-free fiber morphology with a small fiber diameter. In particular, polymer concentration and solvent ratio were found to be the most influential parameters for fiber morphology. After optimization, 20 wt% of polymer concentration, a 2:1 volumetric ratio of ethanol to chloroform, a feed rate

of 1 ml h^{-1}, a voltage of 17 kV, and a needle-collector distance of 13 cm to electrospun P(AAc-co-C18A) hydrogels with varying molar fractions of C18A were selected.

Characterization: For ^{1}H NMR measurements, 10 mg of copolymer sample was carefully dissolved in 0.75 mL of deuterated chloroform ($CDCl_3$). The resulting solution was then carefully transferred to 4 mm NMR tubes. After this preparation, the ^{1}H NMR spectra were obtained using a VNMRS 500 MHz spectrometer (Agilent Technologies, CA, USA). Fourier-transform infrared (FTIR) for both the bulk and electrospun hydrogels were acquired using a Carry 630 FTIR spectrometer (Agilent Technologies, CA, USA). The samples were positioned on an ATR accessory, and the spectral data were collected within the wavenumber range spanning from 4000 to 400 cm^{-1}. Scanning electron microscopy (SEM) was performed using an FEI Quanta FEG 200 microscope (UMass Chan, MA, USA). Fiber size distribution was determined using a previously established image processing method in MATLAB, with detailed procedures available elsewhere.[21] Differential scanning calorimetry (DSC) analyses of the hydrogels before and after the electrospinning process, were performed using a Diamond differential scanning calorimeter (Perkin Elmer, MA, USA). 10 mg of each sample was loaded into aluminum pans and subjected to heating from 0 to 80 °C at a rate of 5 °C min^{-1}. Subsequently, the samples were cooled down to 0 °C at the same rate. To prevent any potential reactivity of the samples with the surrounding environment during the measurements, a continuous flow of nitrogen gas (at a rate of 19.8 mL min^{-1}) was passed over the DSC cell. The swelling ratio (SR) of the printed hydrogels was determined by keeping the hydrogel specimen in water until obtaining the swelling equilibrium, which required about two weeks. SR was calculated by $SR = m_s/m_d$, where m_s and m_d are the weights of the swollen and dry specimen, respectively. X-ray diffraction (XRD) measurements were conducted using a Panalytical Empyrean instrument with Cu-Kα radiation. Data were gathered across the angular range of 2θ from 1° to 50° at a scanning rate of 1° min^{-1}.

The impact of various temperatures on the storage modulus (G') and loss factor (tan δ) of the hydrogels was examined through an oscillatory temperature-sweep test. A disk-shaped sample measuring 20 mm in diameter and 1 mm in thickness was positioned between the parallel plates of a Bohlin Gemini 150 rheometer (Bohlin Instruments, UK). The sample was then subjected to a cooling-heating cycle ranging from 25 to 65 °C at a fixed oscillation frequency of 1 Hz (6.3 rad s^{-1}), and strain amplitude (γ_o) of 0.1%. The melt processability of the hydrogels was evaluated using a frequency sweep test at different temperatures between 55 and 85 °C. A conical plate (40 mm and 4°) was used for this measurement, which is more suitable for molten/liquid samples. The mechanical performance of the electrospun hydrogels was assessed by conducting uniaxial tensile testing using a Zwick Roell Z0.5 TH universal testing machine. A fibrous mat with length of 40 mm, width of 5 mm and thickness of 0.1 mm was subjected to an elongation test at a controlled crosshead speed of 5 mm min^{-1}. The load-elongation curve was recorded using the testXpert III Testing Software from Zwick/Roell. To evaluate shape memory, specimens identical to those used in the tensile tests, 40 mm long and 5 mm wide, were first stretched to twice their original length at a temperature of 65 °C. The specimen was then immediately submerged in water at a temperature of 25 °C under force to maintain its elongated shape. Finally, the specimen was returned to 65 °C to assess the shape-recovery. The shape fixity and shape recovery ratios, R_f and R_r, respectively, were calculated using the equations:

$$R_f = \frac{l_s}{l_t} \times 100 \quad (1)$$

$$R_r = \frac{l_{t-l_r}}{l_{t-l_o}} \times 100 \quad (2)$$

where l_o is the original length of the sample, l_t and l_s are the stretched sample lengths at 25 °C before and after releasing the stress, respectively, and l_r is the length of recovered sample as a result of stimulation at 65 °C.

Supporting Information

Supporting Information is available from the Wiley Online Library or from the author.

Acknowledgements

This research was funded by European Commission Horizon 2020 Marie Skłodowska-Curie Actions Co-fund program, Project No 121C032. The authors also would like to thank Dr. Esra Su, Dr. Berkant Yetiskin, and Dr. Mehmet Emin Pasaoglu for their technical support and/or guidance. O.O. thanks the Turkish Academy of Sciences (TUBA) for the partial support.

Conflict of Interest

The authors declare no conflict of interest.

Data Availability Statement

The data that support the findings of this study are available in the Supporting Information of this article.

Keywords

electrospinning, hydrophobic interaction, melt-processability, polyacrylic acid, shape-memory hydrogels

Received: May 2, 2024
Revised: June 15, 2024
Published online:

[1] E. Su, C. Bilici, G. Bayazit, S. Ide, O. Okay, *ACS Appl. Mater. Interfaces* **2021**, *13*, 21786.
[2] A. S. Kozlenko, I. V. Ozhogin, A. D. Pugachev, M. B. Lukyanova, I. M. El-Sewify, B. S. Lukyanov, *Top. Curr. Chem.* **2023**, *381*, 8.
[3] A. Mukherjee, P. Srivastava, J. K. Sandhu, *Mater. Today: Proc.* **2023**, *81*, 350.
[4] C. Montoya, L. Roldan, M. Yu, S. Valliani, C. Ta, M. Yang, S. Orrego, *Bioact. Mater.* **2023**, *24*, 1.
[5] Z. Hou, X. Liu, M. Tian, X. Zhang, L. Qu, T. Fan, J. Miao, *J. Mater. Chem. A* **2023**, *11*, 17336.
[6] T. Dayyoub, A. V. Maksimkin, O. V. Filippova, V. V. Tcherdyntsev, D. V. Telyshev, *Polymers* **2022**, *14*, 3511.
[7] T. Abdullah, O. Okay, *ACS Appl. Bio Mater.* **2023**, *6*, 703.
[8] U. Gulyuz, O. Okay, *Macromolecules* **2014**, *47*, 6889.
[9] J. Simińska-Stanny, M. Nizioł, P. Szymczyk-Ziółkowska, M. Brożyna, A. Junka, A. Shavandi, D. Podstawczyk, *Addit. Manuf.* **2022**, *49*, 102506.
[10] C. Bilici, V. Can, U. Nöchel, M. Behl, A. Lendlein, O. Okay, *Macromolecules* **2016**, *49*, 7442.
[11] D. C. Tuncaboylu, M. Sari, W. Oppermann, O. Okay, *Macromolecules* **2011**, *44*, 4997.
[12] O. Okay, *J. Mater. Chem. B* **2019**, *7*, 1581.
[13] O. Okay, *Adv. Polym. Sci.* **2020**, *285*, 21.
[14] C. Bilici, S. Ide, O. Okay, *Macromolecules* **2017**, *50*, 3647.
[15] M. Pekař, *Front. Mater.* **2015**, *1*, 35.
[16] G. Huang, Z. Tang, S. Peng, P. Zhang, T. Sun, W. Wei, L. Zeng, H. Guo, H. Guo, G. Meng, *Macromolecules* **2021**, *55*, 156.
[17] M. G. Grewal, C. B. Highley, *Biomater. Sci.* **2021**, *9*, 4228.
[18] Y. Huang, X. Li, Z. Lu, H. Zhang, J. Huang, K. Yan, D. Wang, *J. Mater. Chem. B* **2020**, *8*, 9794.

[19] G. G. de Lima, S. Lyons, D. M. Devine, M. J. Nugent, in *Hydrogels: Recent Advances* (Eds.: V. K. Thakur, M. K. Thakur), Springer, Singapore **2018**, Ch. 9.
[20] X. Wen, J. Xiong, S. Lei, L. Wang, X. Qin, *Adv. Fiber Mater.* **2022**, *4*, 145.
[21] T. Abudula, U. Saeed, N. Salah, A. Memic, H. Al-Turaif, *J. Nanosci. Nanotechnol.* **2018**, *18*, 8240.
[22] A. Refate, Y. Mohamed, M. Mohamed, M. Sobhy, K. Samhy, O. Khaled, K. Eidaroos, H. Batikh, E. El-Kashif, S. El-Khatib, *Heliyon* **2023**, *9*, e17051.
[23] R. Sukowati, B. H. Agung, Y. M. Rohman, M. G. Sabandar, W. X. Waresindo, D. A. Hapidin, D. Edikresnha, K. Khairurrijal, *Mater. Today: Proc.* **2024**, https://doi.org/10.1016/j.matpr.2024.03.009.
[24] G. P. Tamilarasi, G. Sabarees, K. Manikandan, S. Gouthaman, V. Alagarsamy, V. R. Solomon, *Mater. Adv.* **2023**, *4*, 3114.
[25] H. Park, T. V. Patil, S. D. Dutta, J. Lee, K. Ganguly, A. Randhawa, H. Kim, K. T. Lim, *Adv. Healthcare Mater.* **2024**, *13*, 2304114.
[26] Y. Li, J. Wang, Y. Wang, W. Cui, *Composites, Part B* **2021**, *223*, 109101.
[27] L. Dong, C. M. Witkowski, M. M. Craig, M. M. Greenwade, K. L. Joseph, *Nanoscale Res. Lett.* **2009**, *4*, 1517.
[28] Y. Geng, X. Y. Lin, P. Pan, G. Shan, Y. Bao, Y. Song, Z. L. Wu, Q. Zheng, *Polymer* **2016**, *100*, 60.
[29] D. K. Doguscu, C. Alkan, *Int. J. Eng. Appl. Sci.* **2015**, *2*, 257962.
[30] B. Elarbe, I. Elganidi, N. Ridzuan, K. Yusoh, N. Abdullah, S. Vijayakumar, *J. Pet. Explor. Prod. Technol.* **2022**, *12*, 1811.
[31] I. Woodward, W. Schofield, V. Roucoules, J. Badyal, *Langmuir* **2003**, *19*, 3432.
[32] M. Olukman Şahin, C. Demirbilek Bucak, *J. Polym. Environ.* **2023**, *31*, 3650.
[33] F. Snijkers, D. Vlassopoulos, *J. Rheol.* **2011**, *55*, 1167.
[34] N. A. Nguyen, S. H. Barnes, C. C. Bowland, K. M. Meek, K. C. Littrell, J. K. Keum, A. K. Naskar, *Sci. Adv.* **2018**, *4*, 4967.
[35] L. Zhang, W. Ma, H. Tang, Y. Yu, L. Wang, T. Li, Z. Fang, Z. Qiao, *Chem. Eng. J.* **2023**, *466*, 143332.
[36] S. Ramakrishna, *An Introduction to Electrospinning and Nanofibers*, World Scientific, Singapore **2005**.
[37] C. Mit-uppatham, M. Nithitanakul, P. Supaphol, *Macromol. Chem. Phys.* **2004**, *205*, 2327.
[38] Z. Sun, J. M. Deitzel, J. Knopf, X. Chen, J. W. Gillespie Jr., *J. Appl. Polym. Sci.* **2012**, *125*, 2585.
[39] J. Konieczkowska, A. Wasiak, A. Sobolewska, S. Bartkiewicz, J. G. Małecki, E. Schab-Balcerzak, *J. Photochem. Photobiol., A* **2023**, *444*, 114979.
[40] P. Linstorm, *J. Phys. Chem. Ref. Data, Monograph* **1998**, *9*, 1.
[41] H. Okuzaki, K. Kobayashi, F. Hishiki, S.-J. Su, H. Yan, *J. Nanosci. Nanotechnol.* **2011**, *11*, 5193.
[42] S. Deng, J. Yao, H. Bai, H. Xiu, Q. Zhang, Q. Fu, *Polymer* **2021**, *224*, 123736.
[43] T. Ghosh, T. Das, R. Purwar, *Polym. Eng. Sci.* **2021**, *61*, 1887.
[44] P. Gupta, R. Purwar, *J. Polym. Res.* **2020**, *27*, 296.
[45] F. Zhang, Y. Si, J. Yu, B. Ding, *Chem. Eng. J.* **2023**, *456*, 140989.
[46] T. D. Lu, Q. Wang, S. S. Gu, S. P. Sun, *Adv. Funct. Mater.* **2024**, *34*, 2310218.
[47] U. Stachewicz, R. J. Bailey, W. Wang, A. H. Barber, *Polymer* **2012**, *53*, 5132.
[48] X.-X. Wang, G.-F. Yu, J. Zhang, M. Yu, S. Ramakrishna, Y.-Z. Long, *Prog. Mater. Sci.* **2021**, *115*, 100704.
[49] L. Liu, W. Xu, Y. Ding, S. Agarwal, A. Greiner, G. Duan, *Compos. Commun.* **2020**, *22*, 100506.
[50] M. Bao, X. Lou, Q. Zhou, W. Dong, H. Yuan, Y. Zhang, *ACS Appl. Mater. Interfaces* **2014**, *6*, 2611.
[51] P. Nayak, A. K. Ghosh, N. Bhatnagar, *Fibers Polym.* **2023**, *24*, 3421.
[52] X. Wei, L. Chen, Y. Wang, Y. Sun, C. Ma, X. Yang, S. Jiang, G. Duan, *Chem. Eng. J.* **2022**, *433*, 134258.